SLOWNESS SURFACES AND ENERGY FOCUSING PATTERNS OF AUXETIC CUBIC MEDIA

T. PASZKIEWICZ[1], M. PRUCHNIK[2] AND S. WOLSKI[1]

[1] *Chair of Physics, Rzeszów University of Technology*
W. Pola 2, PL-35-959 Rzeszów, Poland

[2] *Institute of Theoretical Physics University of Wrocław*
Pl. Maxa Borna 9, PL-50-204 Wrocław, Poland

Abstract: We study properties of slowness surfaces and energy focusing patterns of cubic elastic media. We restricted ourselves to the region of the stability triangle where Poisson's ratio σ_p of the specimen stretched in the [001] direction and measured for [100] is negative, *i.e.* we consider *all* cubic auxetic materials. We study properties of surfaces and energy focusing patterns for *all* elastic auxetic media characterized by $\sigma_p = -1/3$.

1. INTRODUCTION

Recently there is considerable interest in auxetics - elastic materials with negative Poisson's ratio (cf. [1-3]). Generally the calculation of Poisson's ratio is complicated for directions oblique to the crystal axes [4]. Therefore, in our previous papers [5, 6] we restricted ourselves to Poisson's ratio for [001] stretch measured for [100] lateral direction and established the region of the stability triangle (ST) (cf. [6]) where the mentioned Poisson's ratio is negative. We shall underline that the characteristics of particular region of auxeticity depends on the choice of the stretch direction **n** and the direction **m** of measurement [7]. To indicate this dependence we shall use notation **nm**-auxeticity region of ST.

The present paper is devoted to the study of geometrical properties of slowness surfaces of long wavelength acoustic phonons [8, 9] in the [001][100]-auxeticity region (for simplicity we shall use a short notation zx-Poisson's ratio and zx-auxeticity region). We also obtained the energy focusing patterns [8, 9] which are images of these surfaces under the mapping induced by phonon focusing, which is mathematically known as the Gauss maps (cf. [10]). These maps are obtained in time-of-flight experiments with ballistic phonon beams [8, 9].

2. CHOICE OF ELASTICITY PARAMETERS

2.1. Partition of the stability triangle

Within the framework of theory of elastic media, in a chosen Cartesian coordinate system, the phase c and group velocities **v**, as well as polarization vectors **e** of long wavelength acous-

tic phonons depend on parameters characterizing elastic properties of the medium. The most commonly used is the set of elastic constants $\{C_{ij}: i, j = 1, 2, 3\}$ and the mass density ρ. However, following Every [11], in our previous papers [12, 13] for cubic crystals we used a linear combination of C_{11} and C_{44}

$$s_1 = (C_{11} + 2C_{44}), \tag{1}$$

and two dimensionless parameters s_2, s_3

$$s_2 = \frac{(C_{11} - C_{44})}{s_1}, \qquad s_3 = \frac{(C_{11} - C_{12} - 2C_{44})}{s_1}. \tag{2}$$

Notice that the triple (s_1, s_2, s_3) is equivalent to the set (C_{11}, C_{12}, C_{44}) of elastic constants. Since the parameter s_3 vanishes for isotropic media, we shall call it the elastic anisotropy parameter. The parameter s_1 is a scaling parameter. The phase and group velocities are proportional to it. The Poisson ratio does not depend on s_1.

We shall remind that elastic properties of all media belonging to the cubic crystallographic system, *i.e.* to the crystallographic classes 23 *(T)*, $\overline{4}3m$ *(T$_d$)*, *m3* *(T$_h$)*, 432 *(O)* and *m3m* *(O$_h$)*, are described by the same set of parameters of elasticity.

The condition of mechanical stability imposes certain restrictions on values of the parameters s_1, s_2 and s_3. Namely, s_1 should be positive and

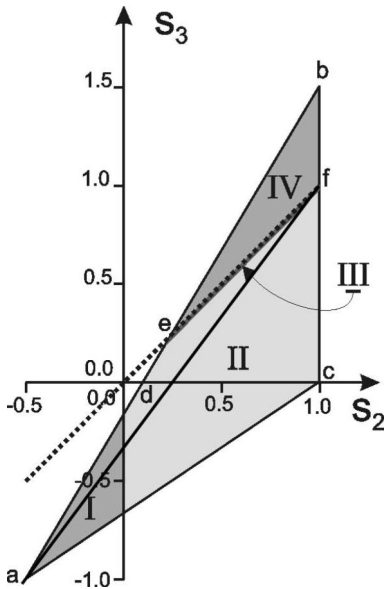$$(1 + 2s_2) > |4s_2 - 3s_3 - 1|, \quad (10s_2 - 6s_3) > 1, \quad s_2 < 1. \tag{3}$$

Fig. 1. Various regions of the stability triangle *abc*. The polarization anomalies line (PAL) $s_2 = s_3$ *(i.e.* $C_{12} = -C_{44}$) is indicated (the dotted line). The line $s_2 = 0$ is called the vertical polarization anomalies line (VPAL) [5]. On the *af*-line the *zx*-Poisson ratio attains the value 0

These inequalities mean that s_2 and s_3 can only vary inside the stability triangle (*abc* triangle in Fig. 1) bounded by $s_3 = \frac{5}{3}s_2 - \frac{1}{6}$ (*ab*-side), $s_3 = \frac{2}{3}s_2 - \frac{2}{3}$ (*ac*-side) and $s_2 = 1$ (*bc*-side) lines.

As we shown [5], the stability triangle *abc*, can be divided into four separate regions in which corresponding crystalline media exhibit different acoustic properties. These regions are shown in Fig. 1. The region I is lying left to the s_3 axis, *i.e.* for it $s_2 < 0$. We shall call the line $s_2 = 0$ the vertical polarization anomalies line (VPAL). The region II is located between VPAL and the line which we call the polarization anomalies line (PAL), which lies slightly below the acoustic anomalies line (AAL), *i.e.* $s_3 = s_2$ line. The PAL can be found only numerically, and not necessarily is straight. The region III is placed between PAL and AAL, while region IV is a part of the stability triangle lying above AAL.

2.2. *zx*-Poisson's ratio

Consider the dependence of the *zx*-Poisson ratio σ_p on parameters of elasticity

$$\sigma_p = \frac{C_{12}}{C_{11} + C_{12}} = \frac{(4s_2 - 3s_3 - 1)}{3(2s_2 - s_3)}. \tag{4}$$

The *zx*-Poisson ratio σ_p vanishes for $C_{12} = 0$, i.e. on the section $\overline{af}$ of $s_3 = \frac{1}{3}(4s_2 - 1)$ line. Above this line σ_p is negative while below it is positive. According [14] in the case of cubic intermediate valent compounds the vanishing σ_p indicates the semiconductor-metal transition. Plot of σ_p is presented in Fig. 2.

We shall underline that the region of auxeticity (cf. also Fig. 3) forms a finite part of the stability triangle, *i.e.* defines a continuous set of finite measure of cubic auxetic compounds. Hence, one may expect that auxeticity could be a common phenomenon.
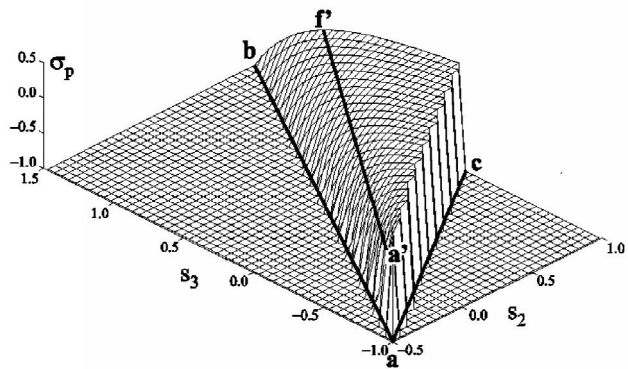

Fig. 2. Dependence of the *zx*-Poisson ratio σ_p on s_2 and s_3. On $\overline{a'f'}$ the Poisson ratio vanishes. Left to $\overline{af}$ (the projection of $\overline{a'f'}$ onto the plane $\sigma_p = -1.0$), hence $\sigma_p < 0$ also on $\overline{ab}$. Right to $\overline{af}$ $\sigma_p > 0$

In Sect. 3.3 we shall study properties of slowness surfaces in *zx*-region of auxeticity along a line of constant value of σ_p.

From Eq. 4 it follows that the parameters s_2 and s_3 are related by a linear relation

$$s_3 = \frac{2(2-3\sigma_P)}{3(1-\sigma_P)} s_2 - \frac{1}{3(1-\sigma_P)}. \tag{5}$$

From Eq. 5 it follows that to the borders of auxeticity region correspond to $\sigma_p = 0$ (the line af in Fig. 1) and $\sigma_p = -1$ (the *ab*-side of the stability triangle (cf. Fig. 1)).

3. PROPERTIES OF LONG-WAVELENGTH ACOUSTIC PHONONS

Weakly disturbed states of crystalline lattices can be described in terms of phonons. Here we consider only long wavelength acoustic phonons (LAPs) - fast ($j = 0$), slow ($j = 1$) and medium ($j = 2$) [11]. As a rule the fast mode is quasilongitudinal and the remaining modes are quasitransverse. However, there exists regions on ST and directions for which $j = 0$ mode is quasitransverse and at least one of the remaining modes is quasilongitudinal [5] (cf. also Sect. 3.4).

3.1. Phase and group velocities of long-wavelength phonons

A phonon carries the energy $\varepsilon = \hbar\omega$ and quasimomentum $\mathbf{p} = \hbar\mathbf{q}$. The energy ε and, of course, the frequency ω, depend on the wave vector $\mathbf{q}$ and on the index j. The dispersion law of LAPs is linear in the magnitude q of the wave vector

$$\omega(\mathbf{q}, j) = c(\mathbf{q}, j) q \qquad (j = 0,1,2). \tag{6}$$

The coefficient c, called the phase (sound) velocity, depends only on the polarization j and the direction of the wave vector $\hat{\mathbf{q}}$ (or on the angles θ_q and ϕ_q). We shall use a brief notation $Q \equiv (\mathbf{q}, j)$ and $\hat{Q} \equiv (\hat{\mathbf{q}}, j)$.

For long wavelength acoustic phonons the group velocity also depends only on $\hat{Q}$. The group velocity vector

$$v_\alpha(\mathbf{q}, j) = \frac{\partial \varepsilon(\mathbf{p}, j)}{\partial p_\alpha} = \frac{\partial \omega(\mathbf{q}, j)}{\partial q_\alpha}, \tag{7}$$

has the direction of the maximum rate of the frequency change and is perpendicular to a j-th sheet of surface of constant frequency (ω - surface), which is defined as

$$\omega(\mathbf{q}, j) = \omega_0 \qquad (\omega_0 = \text{const}, \quad j = 0, 1, 2). \tag{8}$$

3.2. Local geometrical characteristics of slowness surfaces

Having the phase velocity $c(\hat{Q})$ one can introduce the slowness $s(\hat{Q})$, namely

$$s(\hat{Q}) = c^{-1}(\hat{Q}). \tag{9}$$

The slowness $s(\hat{Q})$ of LAPs depends on $\hat{Q}$ and on parameters of elasticity.

For each j the polar plot of the slowness gives a slowness surface (SlS). For LAPs the equation of a slowness surface is equivalent to

$$\mathbf{q}_j = s\left(\hat{Q}\right)\omega_0\hat{\mathbf{q}} \qquad (j=0,1,2). \tag{10}$$

For each j the constant frequency surface, or constant energy surface, is similar to the corresponding slowness surface. Thus, an ω-surface of LAPs of j-th branch has the same shape as the corresponding slowness surface. Each slowness surface has the symmetry of the considered crystalline medium and generally a *nonspherical shape*. Similarly as the Fermi surface of metals, the slowness surfaces plays a distinguished role in transport phenomena in gases of LAPs. Further we shall term $j = 0$ SIS - the inner sheet, $j = 1$ SIS - the outer sheet, and $j = 2$ - the middle sheet.

Assume that long wavelength phonons are radiated in form of very short pulses by a point source located at the origin of a Cartesian coordinate system. An energy sensitive detector (a bolometer) is placed at the point $\mathbf{r} = (r, \theta_r, {}_r)$ lying in a plane with a normal $\hat{\mathbf{n}}$. A phonon with the wave vector $\mathbf{q} = (q, \theta_q, {}_q)$ falls onto the detector if its group velocity direction $\hat{\mathbf{v}}(\theta_v^{(j)}, \phi_v^{(j)})$ coincides with the direction of the radius vector $\mathbf{r}$ of the detector. Generally, due to the complicated nonspherical shape of surfaces of constant energy, there is more than one solution to the vectorial equation

$$\hat{\mathbf{r}}(\theta_r, \phi_r) = \hat{\mathbf{v}}_j(\theta_j, \phi_v), \tag{11}$$

or to the two equations for angles

$$\theta_r = \theta_v^{(j)}(\theta_q, \phi_q), \quad \phi_r = \phi_v^{(j)}(\theta_q, \phi_q) \quad (j=0,1,2). \tag{12}$$

Denote them by $\theta_{qj}^{(i)}(\theta_r, \phi_r)$, $\phi_{qj}^{(i)}(\theta_r, \phi_r)$, $(i = 1,2,...,n_j)$. For an arbitrary function F_j of $\hat{\mathbf{r}} \equiv (\theta_r, \phi_r)$ we introduce the notation

$$F_j^{(i)}(\theta_r, \phi_r) \equiv F_j\left[\theta_{qj}^{(i)}(\theta_r, \phi_r), \ \phi_{qj}^{(i)}(\theta_r, \phi_r)\right]. \tag{13}$$

The total density of energy $e_n(\mathbf{r})$ of LAPs falling on a small region around a point $\mathbf{r}$ of the surface with the normal $\hat{\mathbf{n}}$ can be expressed by the focusing (enhancement factor) [12]

$$e_n(\mathbf{r}) = \frac{(\hat{\mathbf{n}} \cdot \hat{\mathbf{r}})\hbar\omega_0}{2\pi r^2} \frac{1}{3} \sum_{j=0}^{2} \sum_{i=1}^{n_j} \mathsf{A}_j^{(i)}(\theta_r, \phi_r). \tag{14}$$

The focusing factor is related to the local geometric characteristics of the suitable slowness-surface at the point of intersection of this surface with the vector $\mathbf{q}$. These local characteristics are the length of the vector $\mathbf{q}$, the angle between $\mathbf{q}$ and v_j and the *Gaussian curvature* Γ_j of the j-th sheet of slowness surface, and

$$\mathsf{A}_j(\theta_j, \phi_q) = \left|(\hat{\mathbf{v}}_j \cdot \hat{\mathbf{q}})\right|\left[\Gamma_j(\hat{\mathbf{q}})q^2\right]^{-1}. \tag{15}$$

On parabolic lines and at flattening points (*e.g.* the points of crossing of parabolic lines) of an slowness surface the Gaussian curvature vanishes, hence at such points the densities of energy and of quasimomentum are singular.

3.3. Slowness surfaces in *zx*-auxetic region

Assume that $\sigma_P = -1/3$. To this value of the *zx*-Poisson's ratio it corresponds the line

$$s_3 = \frac{3}{2} s_2 - \frac{1}{4}. \tag{16}$$

The $\sigma_P = -1/3$-line defined by Eq. (16) lies in the middle of the *zx*-auxeticity region (cf. Fig. 3). We distinguished on this line seven points indicated in Fig. 3.
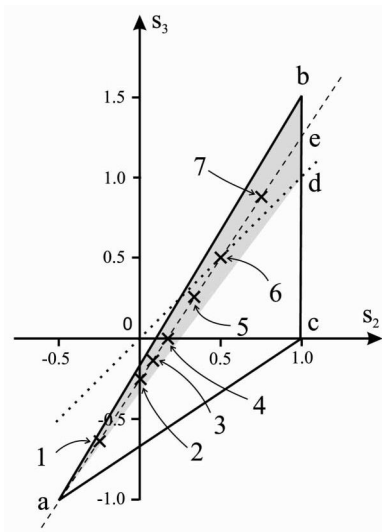
Fig. 3. Cubic crystals are mechanically stable for $s_1 > 0$ and for s_2 and s_3 belonging to the triangle *abc*. In the shaded region $C_{12} < 0$. The interval $\overline{0c}$ (isotropy line) represents stable isotropic media. The dotted line is the polarization anomalies line. The dashed line is defined by Eq. (16). Points of the *zx*-auxeticity region for which slowness surfaces and energy focusing patterns are calculated are indicated by × sign

Notice that the line given by Eq. (16) crosses all four regions shown in Fig. 1. In our previous paper [5] we studied selected properties of SlS in all these regions of ST. Hence we can make reference to results obtained there.

In the regions II and III of the stability triangle the middle (Σ_2) and the outer (Σ_1) surfaces touch each other tangentially in the <100> and conically in the <111> directions. The inner sheet Σ_0 is completely separated from the remaining two sheets. In the region I the behavior of the slowness surfaces is different. For example on VPAL ($s_2 = 0$) Σ_0 makes tangential contact with the Σ_1 and the Σ_2 along <100> directions, while Σ_1 and Σ_2 sheets touch each other at <100> and conically in <111> directions (cf. Fig. 4). Situation in the region IV is opposite - Σ_0 and Σ_2 sheets meet conically in directions of threefold symmetry axes, while Σ_1 and Σ_2 tangentially in directions of fourfold ones.

On AAL line Σ_1 and Σ_2 contact not only along the <001> and the <111>, but also along whole lines connecting these and equivalent points of the unit sphere. The Σ_0 and Σ_2 sheets

contact along lines connecting the neighboring <111>. Since small changes of elasticity parameters lift these degeneracies along lines (of course leaving unchanged degeneracies along acoustic axes) they are unstable.
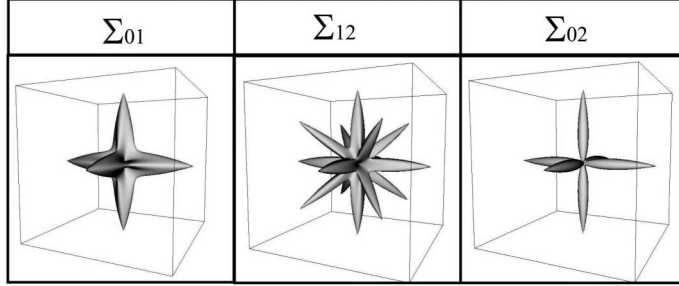

| Σ_{01} | Σ_{12} | Σ_{02} |

Fig. 4. Extremal points of Σ_{ij} surfaces indicate directions in which i and j ($i,j = 1, 2, 3$, $i \neq j$) sheets of SIS touches each other for point no. 2 of the $\sigma_P = -1/3$-line, for which $S_2 = 0.00$, $S_3 = -0.25$. Edges of cubes are directed along <001> rangle directions

The most straightforward way of representing degenerate directions is to calculate surfaces of slownesses difference, *i.e.* calculate $\Delta s_{ij}(\mathbf{n}) = |s_i(\mathbf{n}) - s_j(\mathbf{n})|$ and vectors

$$\Delta s_{ij} = \Delta s_{ij}(\mathbf{n})\mathbf{n} = \left| s_i(\mathbf{n}) - s_j(\mathbf{n}) \right|\mathbf{n}. \tag{17}$$

For given i and j the tips of these vectors defines a surface, which we shall call Δs_{ij}-surface. Because each slowness surface consists of three sheets, for a given crystalline medium there are three different such surfaces, namely Δs_{20}, Δs_{12} and Δs_{10}. From the definition of the Δs_{ij}--surfaces it is obvious that at degenerate directions these surfaces attain the value 0.

The above approach is simple and efficient, but has two disadvantages: it is hard to precisely locate degenerate directions and it is not easy to distinguish between directions in which phase velocities are close and directions in which they are equal. To overcome this difficulty we transformed the Δs_{ij}-surfaces: the global maximum $\Delta s_{ij}^{(\text{max})}$ of a Δs_{ij}-surface is found, and new vectors are introduced

$$\Delta s_{ij}^{(\text{mir})}(\mathbf{n}) = \left\{ \frac{\left[2\Delta s_{ij}^{(\text{max})} - \Delta s_{ij}(\mathbf{n}) \right]}{2\Delta s_{ij}^{(\text{max})}} \right\}^5 \mathbf{n}. \tag{18}$$

For each pair (i, j) the tips of these vectors form a surface which we shall call Σ_{ij}-surface. In fact these new surfaces are normalized mirror images of the Δs_{ij}, where the mirrors are spheres of radii $\Delta s_{ij}^{(\text{max})}$. Note that for degenerate directions the $\Delta s_{ij}^{(\text{mir})}$ reach the global maxima equal exactly to 1.

We built a program which calculates and depicts Σ_{ij}-surfaces and additionally we implemented techniques which allows one to establish their polar coordinates. Results obtained with this program for the point no. 2 of the $\sigma_P = -1/3$-line are presented in Fig. 4.

Table 1. Sheets of slowness surface for cubic elastic media for all long wavelength acoustic phonons in points nos. 1-7 of $\sigma_P = -1/3$ line. In fact various sheets differ by linear dimensions. Regions where $\Gamma < 0$ are shaded. Regions with positive Gauss curvature are white. The borders of these regions indicate lines of parabolic points ($\Gamma = 0$)

	S_0	S_1	S_2
Point no. 1 $s_2=-0.25$; $s_3=-0.625$			
Point no. 2 $s_2=0.0$; $s_3=-0.25$			
Point no. 3 $s_2=0.083$; $s_3=-0.125$			
Point no. 4 $s_2=0.167$; $s_3=0.0$			
Point no. 5 $s_2=0.333$; $s_3=0.25$			
Point no. 6 $s_2=0.5$; $s_3=0.5$			
Point no. 7 $s_2=0.75$; $s_3=0.875$			

Results of more systematic calculations of the slowness surfaces are presented in Table 1. The curvature of regions of slowness surfaces are indicated: shaded regions have negative, whereas white regions - positive Gauss curvature. Therefore, on lines separating them $\Gamma = 0$. They are called lines of parabolic points.
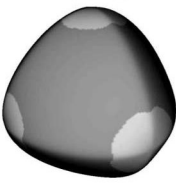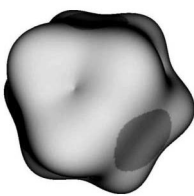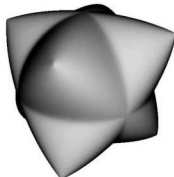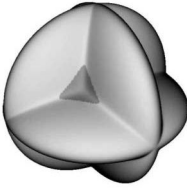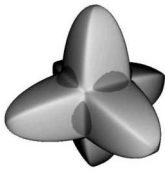
We notice that the SIS of fast phonons (Σ_0) have no lines of parabolic points. When one approaches VPA line (Fig. 3 point no. 2) and PA line (Fig. 3 point no. 7) Σ_0 previously rounded edges becomes sharp, and the Gaussian curvature Γ becomes large. Hence, according formulas (14) and (15), phonons with propagation vectors directed toward points lying on these edges are defocused. Inspection of Table 1 shows that the sheets Σ_1 and Σ_2 have sharp edges too.

The behavior of Σ_1 and Σ_2 sheets is more complicated. On the isotropy line ($s_3 = 0$) outer and inner sheets coincide and all sheets Σ_j ($j = 0, 1, 2$) are perfectly spherical. When one moves along $\sigma_p = -1/3$-line dimples emerge, and next, they develop into furrows. When one changes s_2 and s_3 these dimples evolves - become narrow or broader and within them new structures emerge.

3.4. Behaviour of polarization of phonons

In the case of familiar compounds (as a rule placed in the region II of ST) the fast phonons are quasilongitudinal, whereas slow and medium are quasitransverse. However, with the exception of the region II, there exist directions in which fast phonons are quasitransverse whereas slow and medium phonons are quasilongitudinal. In Table 2 we illustrate this unusual situation for the points no. 1 and 7 of $\sigma_p = -1/3$ line (cf. Fig. 3). Segments of Σ_0 subtending

Table 2. Sheets of slowness surfaces for cubic elastic media for all kinds of LAPs. Various sheets differ by linear dimensions. Polarization anomalies are indicated by grey tones

body angles for which phonons are quasitransverse are indicated by white colour. The remaining gray part of Σ_0 corresponds to quasilongitudinal phonons. Analogously segments of Σ_1 and Σ_2 sheets for which slow phonons are quasilongitudinal are grey, and the remaining part corresponding to transverse phonons are white.

3.5. Energy focusing patterns

From Eqs. (14), (15) it follows that to parabolic lines there corresponds infinite, but integrable energy density e. Lines lying in the chosen plane on which the density of energy transported by phonons is infinite are called caustics. In fact in experiments with ballistic phonon beams mainly caustics are observed. In Table 3 we collected focusing patterns corresponding to slowness surfaces assembled in Table 1. These patterns are obtained with the use of MC AnScat program of Monte Carlo simulations [15]. A bolometer is placed in various points of the plane perpendicular to the z-axis. Regions in which the energy density is large are dark. In white regions $e(\mathbf{r}) = 0$. White structures corresponds to antifocusing parts of Σ_j ($j = 0$, 1, 2). Dark structures reflect the existence of parabolic lines.

3.5.1.   *Polarization   enhancement factors*

For each set $(\hat{\mathbf{n}}, s_2, s_3)$ three mutually perpendicular polarization vectors $\mathbf{e}(\hat{\mathbf{q}}, j; s_2, s_3)$ ($j = 0$, 1, 2) specify a Cartesian set of axes E.

Generally orientation of the introduced set of Cartesian axes is now not arbitrary and changes with $\hat{\mathbf{q}}$, s_2 and s_3. The quantitative characterization of a rotation of $\mathsf{E}(\hat{\mathbf{q}}, s_2, s_3)$ with changing $\hat{\mathbf{q}}$ and with varying elasticity parameters is a quite complicated task [5].

Consider j-th mode for arbitrarily selected values of s_2 and s_3. To characterize the rate of change of E we introduce the enhancement factor $\mathsf{A}_e(\hat{Q})$ resembling the familiar enhancement factor for the group velocity (15). Let us choose a bundle of wave vectors around $\hat{\mathbf{q}}$ subtending the solid angle $\Delta\Omega_q(\hat{\mathbf{q}})$. To this bundle there corresponds a bundle of polarization vectors around $\mathbf{e}(\hat{Q})$ subtending the body angle $\Delta\Omega_e^{(j)}(\hat{\mathbf{q}})$. We may regard $\mathsf{A}_e(\hat{Q})$ as the limit of the ratio of solid angles $\Delta\Omega_q(\hat{\mathbf{q}})$ and $\Delta\Omega_e^{(j)}(\hat{\mathbf{q}})$ when $\Delta\Omega_q(\hat{\mathbf{q}}) \to 0$

$$\mathsf{A}_e^{(j)}(\hat{Q}) \equiv \lim_{\Delta\Omega_q(\hat{\mathbf{q}}) \to 0} \frac{\Delta\Omega_q(\hat{\mathbf{q}})}{\Delta\Omega_e^{(j)}(\hat{\mathbf{q}})}. \tag{19}$$

Since for each j the field of polarization vectors is not potential $(\mathrm{rot}_q \mathbf{e}(\hat{Q}) \neq 0)$, a closed surface perpendicular to set of polarization vectors $\mathbf{e}(\hat{Q})$ $(\hat{\mathbf{q}} \in 4\pi)$ does not exist. This means that, differently than the enhancement factors of the group velocity, the polarization enhancement factors $\mathsf{A}_e(\hat{Q})$ are *not* related to local geometrical characteristics of some surfaces (such as, for example, the Gaussian curvature).

Using our program [15] we performed Monte Carlo experiments and obtained maps of $A_e(\hat{Q})$ for cubic auxetic media defined by points no. 1-7 on the $\sigma_p = -1/3$-line. They are shown in Table 4.

Table 3. Energy focusing patterns corresponding to SIS gathered in Table 1. Gray tones reflect value of energy density $e(\mathbf{r})$. Regions where $e(\mathbf{r})$ is large are intensively dark. Dark structures are caustics reflecting the presence of lines of parabolic points. White structures corresponds to regions antifocusing parts of Σ_j ($j = 0,\ 1,\ 2$) where Γ is large

Table 4. The (θ_e, ϕ_e) maps of the polarization enhancement factors for all j modes and all points of the $\sigma_p = -1/3$-line. Dark regions correspond to large enhancement factors. The darkness scale of different patterns is not the same
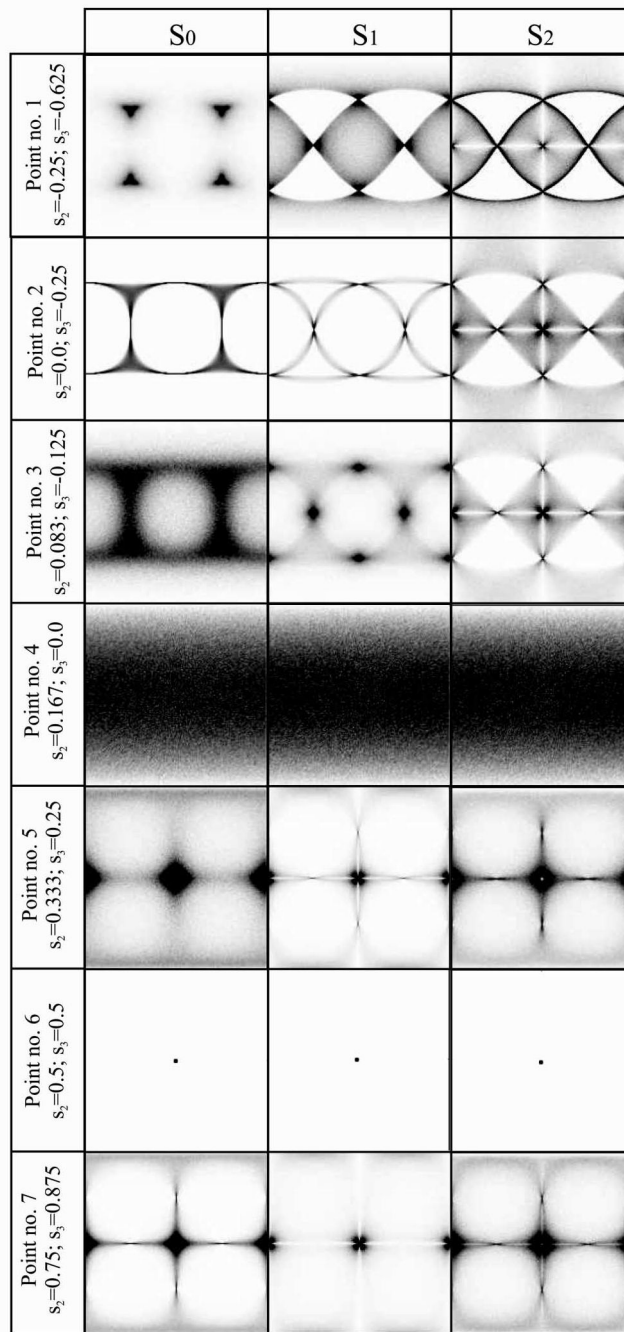
The <001> axes are represented by a points located in the center of the square-shaped region of the polar and azimuthal angles, by the centers of their vertical sides and by whole horizontal sides (cf. patterns belonging to the sixth row of Table 4). Three-leaf clovers seen in the first pattern of the first row surround the <111>. Spots seen in the second element of the third row are centered around [110] and the equivalent directions (four of them are placed on vertical sides of the square). All "caustic" lines which are seen in patterns from Table 4 join high symmetry directions. In all regions there exist white "districts" where polarization vectors are strongly defocused. When moving toward AAL a very strong focusing of polarization vectors is observed in <100> directions (sixth row of Table 4). This is in agreement with observation that on AAL these vectors are fixed along fourfold symmetry axes. One should underline that intensities of various patterns depicted in Table 4 differ immensely.

References

[1] R. H. Baughman, *Auxetic materials: Avoiding the shrink,* Nature **425**, 667-670 (2003).

[2] R. S. Lakes and R. Witt, *Making and Characterizing Negative Poisson's Ratio Materials,* International Journal of Mechanical Engineering Education **30**, 50 (2002).

[3] K. E. Evans and A. Alderson, *Auxetic materials: functional materials and structures from lateral thinking,* in: Advanced Materials (Weinheim, Germany) **12**, 617-628 (2000).

[4] R. H. Baughman, J. M. Shacklette, A. A. Zakhidov, and S. Stafström, *Negative Poisson's ratios as a common feature of cubic metals,* Nature **392**, 362-365 (1998).

[5] T. Paszkiewicz and M. Pruchnik, *Acoustic phonons in cubic media: properies of their polarizations and the diffusion coefficient,* Eur. Phys. J. B **24**, 91-99 (2001).

[6] T. Paszkiewicz, M. Pruchnik, and P. Zieliński, *Unified description of elastic and acoustic properties of cubic media: elastic instabilities, phase transitions and soft modes,* Eur. Phys. J. B **24**, 327-338 (2001).

[7] T. Paszkiewicz, M. Pruchnik, and S. Wolski, *Anisotropy of elastic characteristics of cubic media,* in preparation.

[8] J. P. Wolfe, *Imaging Phonons. Acoustic Wave Propagation in Solids,* Cambridge University Press, Cambridge, 1998.

[9] T. Paszkiewicz and M. Pruchnik, *Kinetic description of the phonon-pulse propagation and phonon images of crystalline solids,* Physica **232**, 747-768 (1996).

[10] D. Arbruster and G. Dangelmayr, *Topological singularities,* Z. Phys. B - Condensed Matter, **52**, 87-94 (1983).

[11] A. G. Every, *General closed-form expressions for acoustic waves in elastically anisotropic solids,* Phys. Rev. B **22**, 1746-1760 (1980).

[12] T. Paszkiewicz and M. Wilczyński, *Scattering of long-wavelength acoustic phonons by isotopic impurities. Spectra of the collision integral and diffusion equation for crystalline media with cubic symmetry,* Z. Phys. B **88**, 5-15 (1992).

[13] T. Paszkiewicz and M. Wilczyński, *Influence of isotopic and substitutional atoms on the propagation of phonons in anisotropic media,* in: G. K. Horton, A. A. Maradudin (eds.), *Dynamical Properties of Solids* vol. 7, Phonon Physics, the Cutting Edge, North Holland, Amsterdam, pp. 257-348, 1995.

[14] U Schärer and P. Wachter, *Negative elastic constants in intermediate valent $Sm_xLa_{1-x}S$,* Solid State Commun. **96**, 497-500 (1995).

[15] W. M. Gancza, I. A. Obukhov, T. Paszkiewicz, and B. A. Danilchenko, *Experiments on propagation and elastic scattering of down-converting beams ofphonons,* Comp. Meth. Sci. Techn. **7,** 7-46 (2001).